ACS APPLIED MATERIALS & INTERFACES

Research Article

Cite This: ACS Appl. Mater. Interfaces XXXX, XXX, XXX−XXX

www.acsami.org

Enhanced Light Harvesting in Photovoltaic Devices Using an Edge-Located One-Dimensional Grating Polydimethylsiloxane Membrane

Yeong Jae Kim,[†] Young Jin Yoo,[†] Dong Eun Yoo,[‡] Dong Wook Lee,[‡] Min Seok Kim,[†] Hyuk Jae Jang,[†] Ye-Chan Kim,[†] Jae-Hyung Jang,[†] Il Suk Kang,*[,‡] and Young Min Song*[,†]

[†]School of Electrical Engineering and Computer Science, Gwangju Institute of Science and Technology, 123 Cheomdangwagi-ro, Buk-gu, Gwangju 61005, Republic of Korea

[‡]National Nanofab Center, Korea Advanced Institute of Science and Technology, 291 Daehak-ro, Yuseong-gu, Daejeon 34141, Republic of Korea

Supporting Information

ABSTRACT: In streamlined multipurpose applications for light management and protection, encapsulants are merged with photonic crystal structures into solar modules. We present an edge-located 1D grating, attachable polymer on the top of a photovoltaic module to provide a strategy for capturing solar light and improving cell efficiency. Large-area solar arrays suffer from space utilization problems due to nonactive area. The introduction of periodically patterned gratings with specific geometric range is highly preferred to redirect the light toward photovoltaic active areas. To realize optimized broadband light diffraction for solar devices, the theoretical analysis of one-dimensional line patterned diffraction gratings was performed through wave-optic-based simulation. Based on the experimental results, the replica molding-based patterning method was adopted to fabricate the grating polymer for low-cost thin-film production. Also, we demonstrated enhanced light collection by grating patterned encapsulants with improved current density in comparison to the performance of a flat surface.

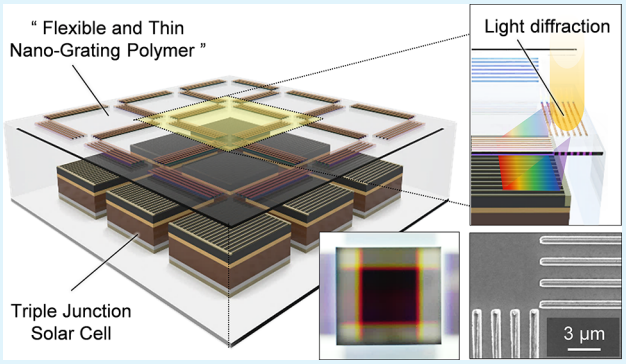

KEYWORDS: *light harvesting, photovoltaic device, diffraction, polydimethylsiloxane, grating structure, soft imprint lithography, encapsulant*

INTRODUCTION

Although mankind's energy production still depends on fossil fuels containing hydrocarbon, such as primary coal, crude oil, and natural gas with limited minable resources, the development of alternative energy resources is attracting enormous interest due to the increasing global energy demand and environmental problems associated with fossil fuels.[1−3] As an alternative source of energy, photovoltaic (PV) devices are widely used to produce electricity utilizing incident sunlight.[4,5] Among the different solar cell types, multijunction solar cells have excellent lifetime/stability and energy conversion efficiency over a broadband solar spectrum with their wide range of terrestrial and space applications.[6−10] In this substantial solar cell industry, the proper approach to protect solar cells from various threats in the external environment, such as chemicals, UV rays, and dust, must be feasibly integrated into the construction of modules. Typically, encapsulants play a key role in solar modules to serve as a protective barrier.[11−14] Moreover, for enhancing solar harvesting, encapsulation materials can be sophisticatedly structured to manage light transmission and deliver light into the active area of solar cells. So far, structural approaches, such as the use of prisms, beer steering coatings, blazed phase gratings, TiO_2 xerogel diffraction gratings, and nanocone arrays, have been reported to improve conversion efficiencies with encapsulants.[15−31] Contrary to fundamental changes in solar cell structures, since encapsulation is the final step in the modularization of solar cells, simple structure and fabrication are required to be close to commercialization. Typically, the diffraction grating structure is one of the candidates meeting this demand, but for practical applications, it is necessary to optimize the grating parameters with diffraction orders and to consider the angular change of the incident light.[30,32−36] Furthermore, for the commercial installation of solar modules, large-scale array formation is inevitable. The conventional module layout consists of a cell array, which generates a blank region that causes power degradation per unit module area. For spatial efficiency, large-area solutions regarding the spacing between PV cell arrays should also be considered.[37−39]

Received: May 29, 2019
Accepted: September 6, 2019
Published: September 6, 2019

DOI: 10.1021/acsami.9b09377
ACS Appl. Mater. Interfaces XXXX, XXX, XXX−XXX

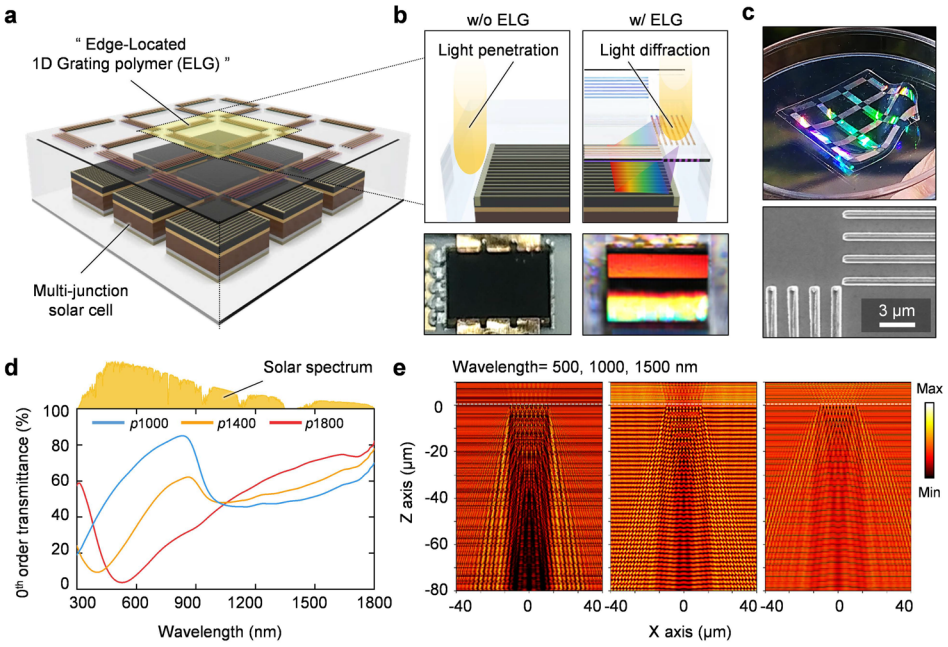

Figure 1. (a) Schematic representation of edge-located 1D grating polymer (ELG) on a photovoltaic cell. (b) Schematic views and photograph images of a w/o ELG and w/ELG on a TJ solar cell. (c) Photograph images of ELG polymer under sunlight and cross section views of SEM image. (d) Zeroth-order transmittance spectra of ELG with periods of 1000, 1400, and 1800 nm. (e) E-field distributions of ELG polymer at 500, 1000, and 1500 nm wavelengths.

Here, we report on an edge-located photonic polymer to capture the unused light that reaches blank areas where electron−hole pair recombination does not take place. Significantly increased optical energy conversion was observed by integrating an edge-located grating polymer that is ultrathin and lightweight. Numerical simulations based on wave optics were performed to determine the spectral properties with three different periodic gratings varying geometric parameters.

In addition, we evaluated the grating diffraction with variation of the grating period to determine the optimal structure for photovoltaic applications. According to theoretical analysis, the edge-located grating is suitable for the light trapping toward solar cell active area which generates electricity. This reduced dead area addresses the solar cell cost issue with light trapping features. Also, our ELG layer can be applicable to other light-capturing structures that have thin and transferable properties.

EXPERIMENTAL SECTION

Optical Simulation. The electric-field intensity and absorption profiles were calculated by employing the finite-difference time-domain (FDTD) modeling. Simulation results for gratings and multijunction solar materials were obtained at a perfectly matched layer boundary with grid spacing of 5 nm in the $x-z$ plane. In the rigorous coupled-wave analysis (RCWA), fifth diffraction order was used to obtain the transmittance spectra and diffracted angle for the PDMS gratings by using RSoft software (Diffract MOD, FullWave, USA). Numerical simulations were conducted with the consideration of material dispersions to calculate wavelength dependencies for the refractive index and extinction coefficients as a function of wavelength (i.e., polydimethylsiloxane polymer and semiconductor materials).[40,41] Furthermore, Monte Carlo ray-tracing simulations were also performed for the navigation of light rays from the air to the solar cell using ZEMAX Optic Studio software (Radiant Zemax LLC, USA).[42]

Optical Characterization. The transmittance spectra for three different grating polymers were obtained with a spectrometer (Agilent-Varian Cary 500, USA), and 1D grating morphologies were achieved by using a scanning electron microscope (SEM, Hitachi S-4700, Japan).

RESULTS AND DISCUSSION

The edge-located 1D grating polymer (ELG) stacked on a PV solar module is illustrated in Figure 1a. The ELG polymer stacked on the top, which provides diffracted light to utilize the unused light on the PV cell array spacing. The conventional PV module consists of a solar cell module covered with silicon resin and transparent grating polymer (Figure 1b, left), and the figure below provides a photograph of it. An ELG layer was stacked onto the solar cell cover to generate diffracted light into the solar cell. The photograph shows that light is diffracted onto the solar cell active area by the ELG layer (Figure 1b, right). To fabricate the line-patterned PDMS polymer, the replica molding method was adopted for low-cost thin-film production. Photographs of the fabricated polymer are presented in the top part of Figure 1c. The thin layer of the structure makes the device flexible and stackable.[26,43,44] Figure 1c, bottom, shows the representative top-view SEM image of the ELG layer. The grating polymer exhibits a low transmittance values in the specific wavelength ranges measured by specular transmittance measurement, which provides the tunable diffraction wavelength by adjustment of the period of the grating structure. (Figure 1d). We note that the polymer with the period of 1800 nm is well matched with the solar spectrum to diffract light with high solar intensity. The dips shift with increasing period. Figure 1e shows the electric field distribution for 1800 nm periodicity obtained by the FDTD method at the 500, 1000, and 1500 nm wavelengths to confirm the enhanced/reduced light intensity over the x-axis. The E-field profiles for the other period of 1000 and 1400 nm are also plotted in Figure S1. The PML boundaries in FDTD help to determine the grating effect individually. The electric-field

DOI: 10.1021/acsami.9b09377
ACS Appl. Mater. Interfaces XXXX, XXX, XXX−XXX

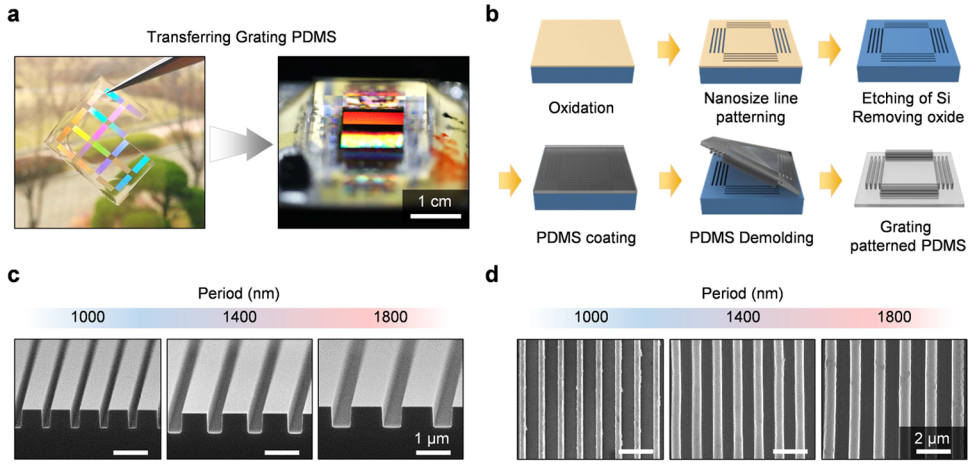

Figure 2. (a) Photographs of fabricated ELG layer and transfer processes onto solar cell device. (b) Fabrication schemes for grating PDMS. (c) 40° tilted SEM images of silicon master mold. (d) Top-view SEM images of the grating patterned PDMS layer.

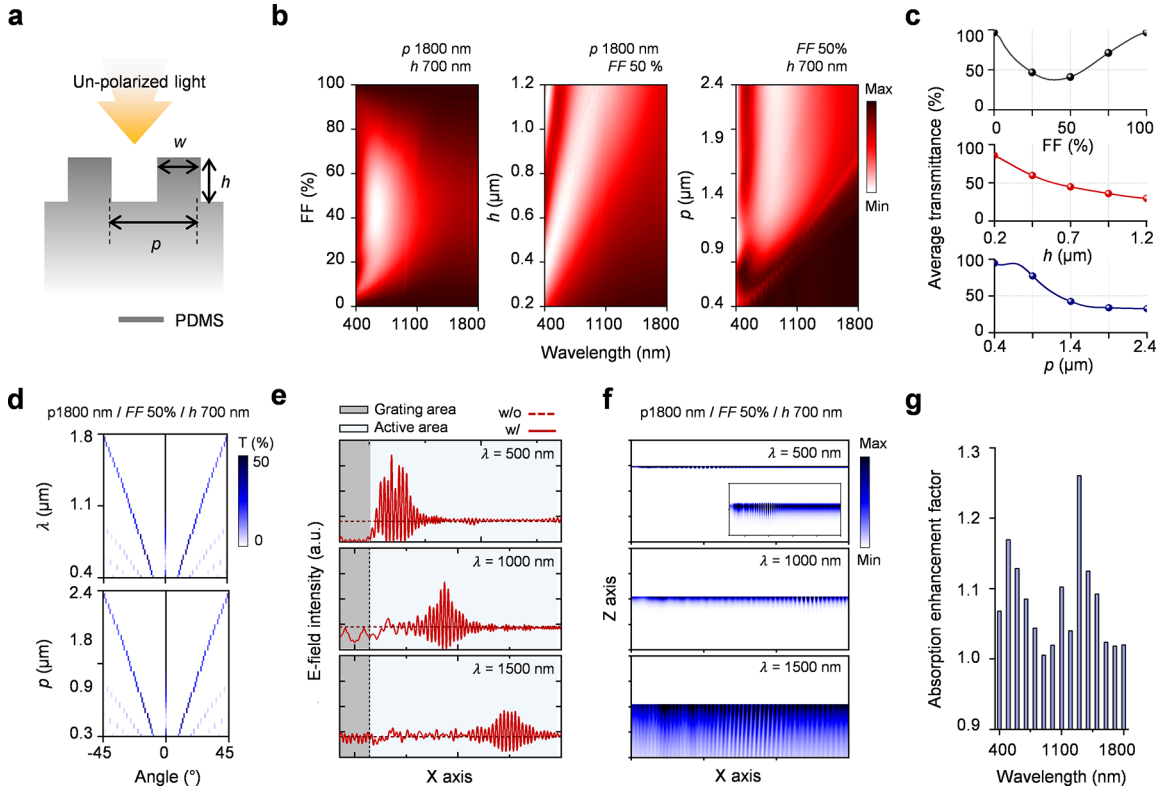

Figure 3. (a) Schematic illustration of a grating PDMS under unpolarized light. (b) Contour plots of zeroth-order transmittance spectra with various filling fractions, heights, and periods. (c) Average zeroth-order transmittance from results calculated in (b). (d) Diffraction angle in the 400−1800 nm wavelength ranges and period from 400 to 2400 at 500 nm wavelengths. (e) Transmitted power versus *x*-axis for diffracted light according to wavelengths of 500, 1000, and 1500 nm. (f) Absorption profiles for triple-junction solar cell. (g) Absorption enhancement factor compared to with and without the ELG layer.

intensity under the grating area is dramatically reduced when strong diffraction occurs at a wavelength of 500 nm. These results show the diffracted light intensities peak at the low zeroth-order transmittance. Thus, the light harvesting at a specific wavelength range can be maximized by designing our proposed structure geometry.

Figure 2a shows the transferring process onto the PV module; we cut the edge of the ELG layer with a razor blade and applied it onto the PV solar module. Figure 2b shows the manufacturing processes for the silicon grating mold. To fabricate the silicon mold, first, a silicon wafer was annealed to form an ∼200 nm thick SiO_2 layer. Then, SiO_2 line arrays with periods of 1000, 1400, and 1800 nm were patterned by the 248 nm wavelength KrF excimer laser scanner (Nikon Inc. NSR-S203B, Japan). The reactive ion etching method was used to anisotropically etch the silicon until ∼700 nm height with a grating patterned SiO_2 mask (RIE, Oxford Plasmalab 133, UK). The fabricated mold was dipped and rinsed with hydrofluoric acid (HF) and deionized (DI) water, respectively, to remove oxide residues. SEM images showing cross section

DOI: 10.1021/acsami.9b09377
ACS Appl. Mater. Interfaces XXXX, XXX, XXX−XXX

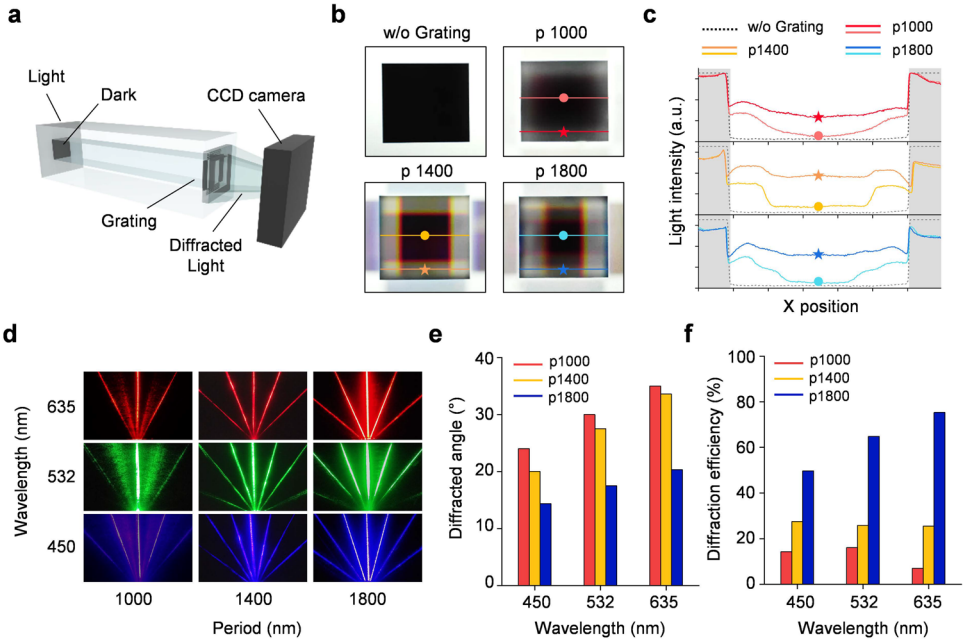

Figure 4. (a) Schematic illustration of measurement set up for light area induced by ELG layer. (b) Photographs of diffracted light according to the grating period. (c) Relative light intensity from CCD camera results. (d) Photographic images of diffracted laser light (wavelength = 450, 532, and 635 nm) passed through the ELG layers. (e) Diffraction angle and efficiency with various grating periods.

views of the fabricated grating silicon with various periods are shown in Figure 2c. After the grating mold was formed, the mold was coated by a release agent to peel off a polymer layer for maintaining grating structure. The base and curing agent of PDMS polymer (Sylgard 184, Dow Corning Corporation, USA) were mixed at a ratio of 5:1. The PDMS mixture was placed onto the vacuum chamber for 30 min for removing entrained air in the polymer, and then the mixture was coated by a spin-coater for 60 s with a speed of 500 rpm on the silicon grating mold. The PDMS layer was cured at 150 °C for 5 min by using a hot plate including natural curing for 3 h at room temperature. Finally, the grating patterned PDMS was peeled off from the mold (Figure 2d). The triple-junction solar cells consisted of 0.7 μm thick $In_{0.5}Ga_{0.5}P$ and 3.65 μm of GaAs on 150 μm of a p-type Ge substrate with three different bandgap energies (i.e., 1.86 eV of InGaP/1.42 eV of GaAs/0.67 eV of Ge). The AlInP window layer was deposited for 30 nm thickness. TiO_2 (50 nm)/Al_2O_3 (50 nm) is coated on top of the solar cell as an antireflective layer (Solapoint Co. Ltd, China). The cell with active area 0.3025 cm^2 was encapsulated by the borosilicate glass (Borofloat33, Schott, Germany) using silicone (Dow DOWSIL 1-2620, Dow Corning, USA) for protective coating. After that, the silicone resin was cured at 150 °C for 30 min. Finally, the PDMS layers were transferred onto encapsulated solar module devices.

Figure 3a shows a one-dimensional grating PDMS polymer for optical calculation. First, the structure geometrical parameters were defined with the period (p), height (h), and filling fraction ($F = 1 - w/p \times 100\%$) to examine the enhanced absorption and diffraction characteristics of the various grating structures. The light diffraction and solar cell absorption of each grating structure were spectrally and spatially investigated (Figure 3b–g). Figure 3b shows the zeroth-order transmittance to find the standard gratings for the broadband wavelength diffraction (400–1800 nm). The filling fraction, period, and height were simulated for the PDMS grating (refractive index, $n_{PDMS} \sim 1.44$) to find the optimized structures for maximizing the light diffraction in the broadband wavelength ranges. The zeroth-order transmittance values were low when the incident light was diffracted. However, the light proceeds mostly in the zeroth order in the case of a subwavelength structure.[44−46] These transmittance calculations were conducted by varying the geometric parameters as a function of wavelength as follows. The filling fraction was varied from 0 to 100% with fixed period (1800 nm) and height (700 nm). The filling fraction is a crucial factor for diffraction; an F of 40–60% was required to diffract light with broadband wavelengths. We also calculated the height as a function of wavelength which had fixed parameters (i.e., period = 1800 nm and filling fraction = 50%). The low transmittance region (white region) gradually shifted toward longer wavelengths when the height (h) was increased. The 1000 and 1400 nm periodic grating were additionally calculated according to h and F. Furthermore, the high refractive index enables diffraction of a broader optical spectrum (see Figure S2). Then, the period (p) was varied from 400 to 2400 nm with a filling fraction of 50% and a height of 700 nm. The period has to be more than 1400 nm to consider broadband light diffraction. As seen in Figure 1e, the spectral irradiance has the highest values at about 500 nm wavelength light in the standard solar spectra, AM 1.5G direct. To consider solar spectra, the height of grating has to be over 600 nm. The filling fraction had relatively low transmittance values from 20% to 60%. Figure 3c shows the averaged transmittance results from Figure 3b to find grating structures with low average transmittance. The average transmittance values were low when the period was greater than 1400 nm, the height was greater than 700 nm, and the filling fraction was between 23% and 60%. Then, we fixed the grating geometrical parameters such that the period was 1800 nm, the height was 700 nm, and the filling fraction was 50% (Figure 3d–g). The diffraction angle depending on the light wavelength and grating period

DOI: 10.1021/acsami.9b09377
ACS Appl. Mater. Interfaces XXXX, XXX, XXX−XXX

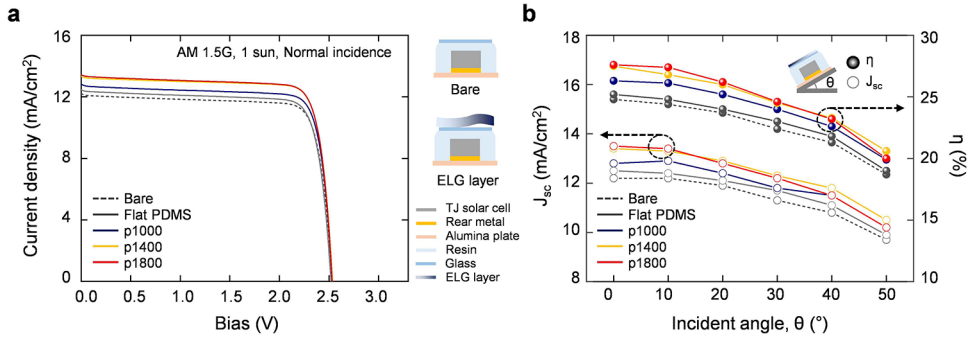

Figure 5. (a) Current density−voltage curves of the triple-junction solar modules and grating PDMS polymers with different periods. (b) Angle of illumination dependencies: short-circuit current J_{sc} (left) and conversion efficiency η (right).

was calculated. The first and second diffraction orders were observed, and the diffraction angle increased proportionally with increasing wavelength (Figure 3d, top). The angle characteristic simulation results are shown in Figure 3d for the grating period at the wavelength of 500 nm with the highest solar irradiance value. When the wavelength had a period similar to the structure, the first order exhibited the highest diffraction efficiency. As the period became larger, the diffraction angle of the light was reduced (see Figure S3). With a small period, only the zeroth order was observed. The diffracted light intensity reached in the solar cell was calculated for wavelengths of 500, 1000, and 1500 nm. The reference light intensity is represented by the dotted line. In the grating area, the light intensity was reduced by the grating structure, and the amount of reduced light was diffracted toward the active area. The enhanced captured light position shifted according to their wavelength. To optimize the grating based on optogeometrical aspect, we simulate the ray-tracing simulating. The ray-tracing simulation results provided the light path in the silicone and PDMS which are attached on the solar cell. The light source was placed outside of the solar cell module (see Figure S4). The optimized diffraction grating for solar cells can be achieved by considering the absorption range of the solar cell material. The absorption profile and enhancement factor were calculated (see Figure 3f,g). In the absorption profile, it was observed that light was absorbed in each absorption layer according to the wavelength variation. The absorption enhancement was increased according to the wavelength range from 400 to 1800 nm, and the overall absorption increased by about 8%. In addition, at a specific wavelength of 1300 nm, the increase rate was more than 20% compared to the conventional structure.

Figure 4a shows the configuration of the captured light measurement for the ELG polymer. To obtain the diffracted light distribution, a light source with a dark square was used, which consisted of the light source, grating layer, and CCD camera. Experiment photographs of the irradiance distribution for various periods are shown in Figure 4b. The light with a dark square passed the grating structure, and it could be observed that the dark regions were reduced by diffracted light. The light coverage increased according to the grating structure due to second-order diffraction, which is matched with the simulation results described above (see Figure 3b). The relative light coverages are presented in Figure 4c; the black dotted line represents the light intensity of flat PDMS polymer for reference data. As shown in the graph, enhanced light intensities were observed for all grating samples. We confirmed that all the gratings had light-capturing properties. Also, it was observed that the light intensity was further strengthened at the corner position by the two grating structures. Figure 4d shows the results obtained from ELG samples with periods of 1000, 1400, and 1800 nm. The diffracted beams were generated by lasers with the three wavelengths of 450, 532, and 635 nm. The transmissive diffraction efficiency is specified by the intensity ratio of the diffracted beam to the initial beam, which is determined according to the shape of the structure as in the preceding simulation results.

To characterize the solar cell parameters such as short-circuit current (J_{sc}), open-circuit voltage (V_{oc}), and fill factor (FF), the current density−voltage (J−V) measurement of the triple-junction modules with various grating PDMS polymers were performed by using a solar simulator with AM 1.5G (Oriel Sol3A, USA) and 1 sun illumination (100 mW/cm^2) at 25 °C (see Figure 5a). The power conversion efficiency (η) was calculated by the following equation:

$$\eta = \frac{J_{sc}\ (\text{mA cm}^{-2}) \times V_{oc}\ (\text{V}) \times \text{FF}\ (\%)}{P_{light}\ (\text{mW cm}^{-2})}$$

To ensure an accurate measurement, a mask cell was used with the aperture size of 1 cm by 1 cm. A forward direction scan was performed in the voltage range from 0 to 3 V (0.15 mV steps) with delaying 1000 ms after forward−reverse scan for five times (Figure S5). The incident light intensity (P_{light}) was calibrated with a Si reference cell (Oriel SRC-1000TC-KG5-N).[48,49] Furthermore, to verify the improvement of efficiency and reliability for our proposed structure, we averaged the measured data of five different devices (Table S1).

The detailed solar cell performances integrated with various ELG layers are summarized in Table 1. The measured J_{sc} was enhanced by employing an ELS layer onto the PV module. As a reference, the solar cell module encapsulated by flat glass was

Table 1. Averaged Solar Cell Parameters for Five Different PV Modules[a]

device	J_{sc} (mA/cm^2)	V_{oc} (V)	FF (%)	efficiency (%)
bare	12.19 (0.04)	2.5 (0)	80.46 (0.05)	24.52 (0.07)
PDMS	12.45 (0.07)	2.5 (0)	80.5 (0.1)	25.05 (0.12)
ELG (p1000)	12.80 (0.05)	2.5 (0)	80.86 (0.09)	25.88 (0.10)
ELG (p1400)	13.33 (0.14)	2.5 (0)	81.42 (0.71)	27.13 (0.19)
ELG (p1800)	13.41 (0.05)	2.5 (0)	80.96 (0.11)	27.15 (0.11)

[a]The standard deviations for each parameter are stated in parentheses (see Table S1).

DOI: 10.1021/acsami.9b09377
ACS Appl. Mater. Interfaces XXXX, XXX, XXX−XXX

measured as 12.19 mA/cm^2. Also, we confirmed the efficiency η improvement due to flat PDMS (J_{sc} = 12.45 mA/cm^2), which is caused by the reduced difference in refractive index between outer environment and PDMS polymer. The J_{sc} value was the highest (13.41 mA/cm^2, 9.09% higher compared to the bare glass) with a period of 1800 nm because it exhibits the most effective zeroth-order transmittance with a broadband spectrum and high-order diffraction. In the optical simulation results, the absorption increased by 1.08 times compared with the existing structure. The efficiency of the solar cell is dependent on the absorption in each layer.[50] In the experimental results, the efficiency increased by 1.07 times from 24.52% to 27.15%, which is similar to the enhancement rate of absorption in the above simulation results.

To analyze the different illumination angle dependency of ELG layer on PV modules, the $J-V$ characteristics were measured in the incident angle (θ) from 0 to 50°. As the θ was increased, the J_{sc} was gradually decreased, and the η was also decreased. However, the ELG encapsulated solar cells exhibited higher J_{sc} and energy conversion efficiency compared to bare glass PV module with incident angle from 0 to 50°. We measured the stability of the efficiencies upon repeated cycle with bare and ELG layer samples (Figure S6). The solar cell efficiency with ELG layer was maintained higher during the repetition compared to bare sample.

CONCLUSIONS

In this work, the light-capturing polymers were designed and applied to photovoltaic modules. The edge-located 1D grating polymer was adopted for redirecting light into the active area of solar cells. The grating periods of 1000, 1400, and 1800 nm are used to generate a high diffraction order and optimize the solar spectrum light intensity. The zeroth-order transmittance for broadband light with high-order diffraction for the grating samples are optimized at the range of filling fraction between 25% and 50%, above a height of 700 nm and a period of 1400 nm. Consequently, it was experimentally found that the improved short-circuit current density was achieved about ~9.09% with the grating period of 1800 nm. In conclusion, the optimized 1D grating polymer provides a higher photovoltaic device efficiency than the bare solar cell device achieved by simply stacking the only grating patterned thin layer without complicated changes of conventional photovoltaic modules. We believe that our light capturing approaches will provide opportunities for encapsulant production of solar-energy-harvesting devices.

ASSOCIATED CONTENT

Supporting Information

The Supporting Information is available free of charge on the ACS Publications website at DOI: 10.1021/acsami.9b09377.

E-field simulations for different grating period; zeroth-order transmittance spectra; diffraction angle with varying wavelength, period, refractive index; ray-tracing simulation results; forward and reverse scan for InGaP/GaAs/Ge triple junction solar cell; stability of the TJ cell efficiency; enhancement of shortcircuit current and power conversion efficiency with optical filter; electrical parameters of different TJ solar modules (PDF)

AUTHOR INFORMATION

Corresponding Authors

*E-mail: ymsong@gist.ac.kr.
*E-mail: iskang@nnfc.re.kr.

ORCID

Yeong Jae Kim: 0000-0002-0870-9044
Young Jin Yoo: 0000-0002-6490-2324
Jae-Hyung Jang: 0000-0001-9633-5574
Young Min Song: 0000-0002-4473-6883

Notes

The authors declare no competing financial interest.

ACKNOWLEDGMENTS

This work was supported by the Korea Institute of Energy Technology Evaluation and Planning (KETEP) and the Ministry of Trade, Industry & Energy (MOTIE) of the Republic of Korea (No. 20183010014310), the National Research Foundation of Korea (NRF) funded by the Korean government (MSIP) (NRF2017M3D1A1039288, 2018H1A2A1060954, and 2018R1A4A1025623), and the GIST Research Institute (GRI) grant funded by the GIST in 2019.

REFERENCES

(1) Shafiee, S.; Topal, E. When Will Fossil Fuel Reserves Be Diminished? *Energy Policy* **2009**, *37*, 181−189.
(2) McGlade, C.; Ekins, P. The Geographical Distribution of Fossil Fuels Unused When Limiting Global Warming to 2 °C. *Nature* **2015**, *517*, 187−190.
(3) Hu, A.; Levis, S.; Meehl, G. A.; Han, W.; Washington, W. M.; Oleson, K. W.; van Ruijven, B. J.; He, M.; Strand, W. G. Impact of Solar Panels on Global Climate. *Nat. Clim. Change* **2016**, *6*, 290.
(4) Dresselhaus, M. S.; Thomas, I. L. Alternative Energy Technologies. *Nature* **2001**, *414*, 332.
(5) Kannan, N.; Vakeesan, D. Solar Energy for Future World:-A Review. *Renewable Sustainable Energy Rev.* **2016**, *62*, 1092−1105.
(6) Takamoto, T.; Washio, H.; Juso, H. Application of InGaP/GaAs/InGaAs Triple Junction Solar Cells to Space Use and Concentrator Photovoltaic. *2014 IEEE 40th Photovoltaic Specialist Conference (PVSC)* **2014**, 0001−0005.
(7) Dimroth, F.; Grave, M.; Beutel, P.; Fiedeler, U.; Karcher, C.; Tibbits, T. N. D.; Oliva, E.; Siefer, G.; Schachtner, M.; Wekkeli, A.; Bett, A. W.; Krause, R.; Piccin, M.; Blanc, N.; Drazek, C.; Guiot, E.; Ghyselen, B.; Salvetat, T.; Tauzin, A.; Signamarcheix, T.; Dobrich, A.; Hannappel, T.; Schwarzburg, K. Wafer Bonded Four-Junction GaInP/GaAs/GaInAsP/GaInAs Concentrator Solar Cells with 44.7% Efficiency. *Prog. Photovoltaics* **2014**, *22*, 277−282.
(8) Yeo, C. I.; Choi, H. J.; Song, Y. M.; Kang, S. J.; Lee, Y. T. A Single-Material Graded Refractive Index Layer for Improving the Efficiency of III−V Triple-Junction Solar Cells. *J. Mater. Chem. A* **2015**, *3*, 7235−7240.
(9) Yamaguchi, M. III-V Compound Multi-Junction Solar Cells: Present and Future. *Sol. Energy Mater. Sol. Cells* **2003**, *75*, 261−269.
(10) Bosi, M.; Pelosi, C. The Potential of III-V Semiconductors as Terrestrial Photovoltaic Devices. *Prog. Photovoltaics* **2007**, *15*, 51−68.
(11) Jang, S.; Kang, S. M.; Choi, M. Multifunctional Moth-Eye TiO_2/PDMS Pads with High Transmittance and UV Filtering. *ACS Appl. Mater. Interfaces* **2017**, *9*, 44038−44044.
(12) Song, H. S.; Yoo, Y. J.; Lee, G. J.; Chang, K. S.; Song, Y. M. Optical Design of Porous ZnO/TiO_2 Films for Highly Transparent Glasses with Broadband Ultraviolet Protection. *J. Nanomater.* **2017**, *2017*, 2738015.
(13) Jørgensen, M.; Norrman, K.; Krebs, F. C. Krebs Stability/Degradation of Polymer Solar Cells. *Sol. Energy Mater. Sol. Cells* **2008**, *92*, 686−714.

DOI: 10.1021/acsami.9b09377
ACS Appl. Mater. Interfaces XXXX, XXX, XXX−XXX

(14) Gao, Y.; Gereige, I.; El Labban, A.; Cha, D.; Isimjan, T. T.; Beaujuge, P. M. Highly Transparent and UV-resistant Superhydrophobic SiO_2-Coated ZnO Nanorod Arrays. *ACS Appl. Mater. Interfaces* **2014**, *6*, 2219−2223.
(15) Kang, E. K.; Yeo, C. I.; Kang, S. J.; Min, J. W.; Song, Y. M.; Lee, Y. T. Improved Light Absorption of GaInP/GaAs/Ge Solar Cell Modules with Micro/Nanoengineered Coverglasses. *IEEE. J. Photovolt.* **2015**, *5*, 1130−1136.
(16) Lee, S. K.; Jeong, H. J.; Kim, Y. C.; Jang, J. H. Improvement in CIGS Solar Cell Efficiency Using a Micro-Prism Array Integrated with Sub-Wavelength Structures. *Sol. Energy Mater. Sol. Cells* **2018**, *186*, 254−258.
(17) Chen, F. H.; Pathreeker, S.; Kaur, J.; Hosein, I. D. Increasing Light Capture in Silicon Solar Cells with Encapsulants Incorporating Air Prisms to Reduce Metallic Contact Losses. *Opt. Express* **2016**, *24*, A1419−A1430.
(18) Leem, J. W.; Choi, M.; Yu, J. S. Multifunctional Microstructured Polymer Films for Boosting Solar Power Generation of Silicon-Based Photovoltaic Modules. *ACS Appl. Mater. Interfaces* **2015**, *7*, 2349−2358.
(19) Choi, K.; Park, S. H.; Song, Y. M.; Lee, Y. T.; Hwangbo, C. K.; Yang, H.; Lee, H. S. Nano-Tailoring the Surface Structure for the Monolithic High-Performance Antireflection Polymer Film. *Adv. Mater.* **2010**, *22*, 3713−3718.
(20) Song, Y. M.; Jang, J. H.; Lee, J. C.; Kang, E. K.; Lee, Y. T. Disordered Submicron Structures Integrated on Glass Substrate for Broadband Absorption Enhancement of Thin-Film Solar Cells. *Sol. Energy Mater. Sol. Cells* **2012**, *101*, 73−78.
(21) Song, Y. M.; Jeong, Y.; Yeo, C. I.; Lee, Y. T. Enhanced Power Generation in Concentrated Photovoltaics Using Broadband Antireflective Coverglasses with Moth Eye Structures. *Opt. Express* **2012**, *20*, A916−A923.
(22) Choi, K.; Yoon, Y.; Jung, J.; Ahn, C. W.; Lee, G. J.; Song, Y. M.; Ko, M. J.; Lee, H. S.; Kim, B. S.; Kang, I. S. Super-Antireflective Structure Films with Precisely Controlled Refractive Index Profile. *Adv. Opt. Mater.* **2017**, *5*, 1600616.
(23) Jeong, H. J.; Kim, Y. C.; Lee, S. K.; Yun, J. H.; Jang, J. H. Enhanced Spectral Response of CIGS Solar Cells with Anti-Reflective Subwavelength Structures and Quantum Dots. *Sol. Energy Mater. Sol. Cells* **2019**, *194*, 177−183.
(24) Jeong, H. J.; Kim, D. S.; Kim, S. B.; Park, C. K.; Yun, J. H.; Jang, J. H. Enhanced Light Absorption in Concentrated GaInP/GaAs/Ge Solar Cells Using a Secondary Optical Element with Subwavelength Structures. *Nanosci. Nanotechnol. Lett.* **2018**, *10*, 413−416.
(25) Kim, D. S.; Jeong, Y.; Jeong, H.; Jang, J. H. Triple-Junction InGaP/GaAs/Ge Solar Cells Integrated with Polymethyl Methacrylate Subwavelength Structure. *Appl. Surf. Sci.* **2014**, *320*, 901−907.
(26) Hwang, I.; Choi, D.; Lee, S.; Seo, J. H.; Kim, K. H.; Yoon, I.; Seo, K. Enhancement of Light Absorption in Photovoltaic Devices Using Textured Polydimethylsiloxane Stickers. *ACS Appl. Mater. Interfaces* **2017**, *9*, 21276−21282.
(27) Fang, C.; Zheng, J.; Zhang, Y.; Li, Y.; Liu, S.; Wang, W.; Jiang, T.; Zhao, X.; Li, Z. Antireflective Paraboloidal Microlens Film for Boosting Power Conversion Efficiency of Solar Cells. *ACS Appl. Mater. Interfaces* **2018**, *10*, 21950−21956.
(28) Kim, D. H.; Dudem, B.; Jung, J. W.; Yu, J. S. Boosting Light Harvesting in Perovskite Solar Cells by Biomimetic Inverted Hemispherical Architectured Polymer Layer with High Haze Factor as an Antireflective Layer. *ACS Appl. Mater. Interfaces* **2018**, *10*, 13113−13123.
(29) Lin, H.; Biria, S.; Chen, F. H.; Hosein, I. D.; Saravanamuttu, K. Waveguide-Imprinted Slim Polymer Films: Beam Steering Coatings for Solar Cells. *ACS Photonics* **2019**, *6*, 878−885.
(30) Gâté, V.; Berthod, L.; Langlet, M.; Vocanson, F.; Verrier, I.; Veillas, C.; Kaminski, A.; Parriaux, O.; Jourlin, Y. Dynamic Interferometry Lithography on a TiO_2 Photoresist Sol-Gel for Diffracting Deflector Module. *J. Nanomater.* **2017**, *2017*, 8548041.
(31) Tavakoli, M. M.; Tsui, K. H.; Zhang, Q.; He, J.; Yao, Y.; Li, D.; Fan, Z. Highly Efficient Flexible Perovskite Solar Cells with Antireflection and Self-Cleaning Nanostructures. *ACS Nano* **2015**, *9*, 10287−10295.
(32) Liu, Y.; Sun, N.; Liu, J.; Wen, Z.; Sun, X.; Lee, S. T.; Sun, B. Integrating a Silicon Solar Cell with a Triboelectric Nanogenerator via a Mutual Electrode for Harvesting Energy from Sunlight and Raindrops. *ACS Nano* **2018**, *12*, 2893−2899.
(33) Park, S.; Heo, S. W.; Lee, W.; Inoue, D.; Jiang, Z.; Yu, K.; Jinno, H.; Hashizume, D.; Sekino, M.; Yokota, T.; Fukuda, K.; Tajima, K.; Someya, T. Self-Powered Ultra-Flexible Electronics via Nano-Grating Patterned Organic Photovoltaics. *Nature* **2018**, *561*, 516−521.
(34) Muchow, M.; Büchner, T.; Sprafke, A.; Seifert, G. Femtosecond Laser-Written High-Efficiency Blazed Phase Gratings in the Volume of Soda Lime Glass for Light Management in Solar Modules. *Opt. Express* **2015**, *23*, 33540−33549.
(35) Na, S. I.; Kim, S. S.; Jo, J.; Oh, S. H.; Kim, J.; Kim, D. Y. Efficient Polymer Solar Cells with Surface Relief Gratings Fabricated by Simple Soft Lithography. *Adv. Funct. Mater.* **2008**, *18*, 3956−3963.
(36) Deng, K.; Liu, Z.; Wang, M.; Li, L. Nanoimprinted Grating-Embedded Perovskite Solar Cells with Improved Light Management. *Adv. Funct. Mater.* **2019**, *29*, 1900830.
(37) Lee, K. T.; Yao, Y.; He, J.; Fisher, B.; Sheng, X.; Lumb, M.; Kang, Y.; et al. Concentrator Photovoltaic Module Architectures with Capabilities for Capture and Conversion of Full Global Solar Radiation. *Proc. Natl. Acad. Sci. U. S. A.* **2016**, *113*, E8210−E8218.
(38) Yoder, M. A.; Yao, Y.; He, J.; Nuzzo, R. G. Optimization of Photon and Electron Collection Efficiencies in Silicon Solar Microcells for Use in Concentration-Based Photovoltaic Systems. *Adv. Mater. Technol.* **2017**, *2*, 1700169.
(39) Li, D.; Li, L.; Jared, B.; Keeler, G.; Miller, B.; Wood, M.; Alford, C.; et al. Wafer Integrated Micro-Scale Concentrating Photovoltaics. *Prog. Photovoltaics* **2018**, *26*, 651−658.
(40) Palik, E. D. *Handbook of Optical Constants of Solids*, 1st ed.; Academic Press: New York, 1985.
(41) Querry, M. Optical Constants of Minerals and Other Materials from the Millimeter to the Ultraviolet (No. CRDEC-CR-88009); Chemical Research Development and Engineering Center, Aberdeen Proving Ground, MD, 1987.
(42) Rubinstein, R. Y.; Kroese, D. P. *Simulation and the Monte Carlo Method*, 3rd ed.; Wiley: New York, 2016.
(43) Kim, Y. J.; Yoo, Y. J.; Lee, G. J.; Yoo, D. E.; Lee, D. W.; Siva, V.; Song, H. S.; Kang, I. S.; Song, Y. M. Enlarged Color Gamut Representation Enabled by Transferable Silicon Nanowire Arrays on Metal-Insulator-Metal Films. *ACS Appl. Mater. Interfaces* **2019**, *11*, 11849−11856.
(44) De Paoli, F. Measuring Polydimethylsiloxane (PDMS) Mechanical Properties Using Flat Punch Nanoindentation Focusing on Obtaining Full Contact. Graduate Theses and Dissertations, University of South Florida, 2015.
(45) Song, Y. M.; Jang, S. J.; Yu, J. S.; Lee, Y. T. Bioinspired Parabola Subwavelength Structures for Improved Broadband Antireflection. *Small* **2010**, *6*, 984−987.
(46) Nam, W. I.; Yoo, Y. J.; Song, Y. M. Geometrical Shape Design of Nanophotonic Surfaces for Thin Film Solar Cells. *Opt. Express* **2016**, *24*, A1033−A1044.
(47) Jing, X.; Ma, J.; Liu, S.; Jin, Y.; He, H.; Shao, J.; Fan, Z. Analysis and Design of Transmittance for an Antireflective Surface Microstructure. *Opt. Express* **2009**, *17*, 16119−16134.
(48) Luber, E. J.; Buriak, J. M. Reporting Performance in Organic Photovoltaic Devices. *ACS Nano* **2013**, *7*, 4708−4714.
(49) Christians, J. A.; Manser, J. S.; Kamat, P. V. Best Practices in Perovskite Solar Cell Efficiency Measurements. Avoiding the Error of Making Bad Cells Look Good. *J. Phys. Chem. Lett.* **2015**, *6*, 852−857.
(50) Sze, S. M. *Physics of Semiconductor Devices*; John Wiley: New York, 1981; pp 22−129.

DOI: 10.1021/acsami.9b09377
ACS Appl. Mater. Interfaces XXXX, XXX, XXX−XXX